Electronic Supplementary Material (ESI) for Nanoscale.

Supporting Information

Chinese ink: a programmable, dual-responsive and self-sensing actuator using a healing-assembling method

Jian Lin[a,b,c], Peidi Zhou[a,b,c], Zhiyuan Wen[a,b], Wei Zhang[a,b,c] , Zhiling Luo[a,b,c] and Luzhuo Chen*[a,b,c]

[a] Fujian Provincial Key Laboratory of Quantum Manipulation and New Energy Materials, College of Physics and Energy, Fujian Normal University, Fuzhou, 350117, China.

[b] Fujian Provincial Collaborative Innovation Center for Advanced High-Field Superconducting Materials and Engineering, Fuzhou, 350117, China.

[c] Fujian Provincial Engineering Technology Research Center of Solar Energy Conversion and Energy Storage, Fuzhou, 350117, China.

*E-mail: ChenLZ@fjnu.edu.cn

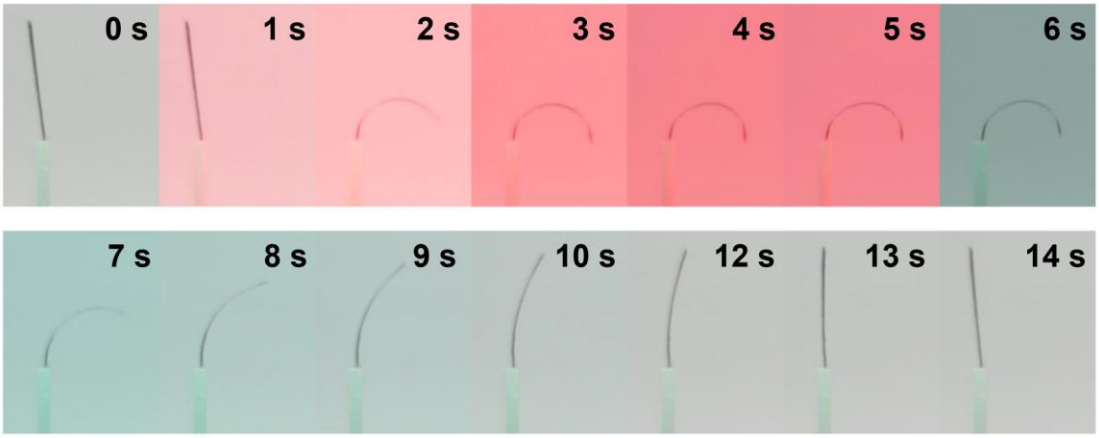

Fig. S1. Light-driven actuation of the ink/GO actuator under NIR light irradiation (400 mW cm^{-2}).

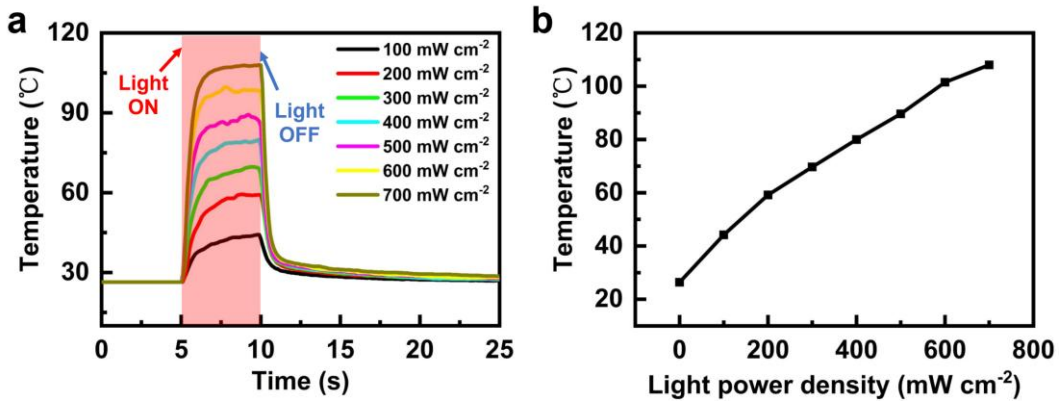

Fig. S2. Temperature change of ink/GO actuator under different NIR light powers. (a) Temperature of ink/GO actuator as a function of time under different NIR light powers (irradiation time is 5 s); (b) Maximal temperature of the ink/GO actuator as a function of light power density.

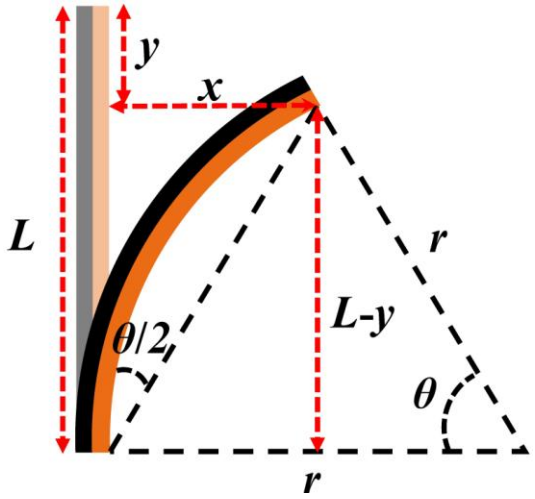

Fig. S3. Analysis of the deformation of ink/GO actuator.

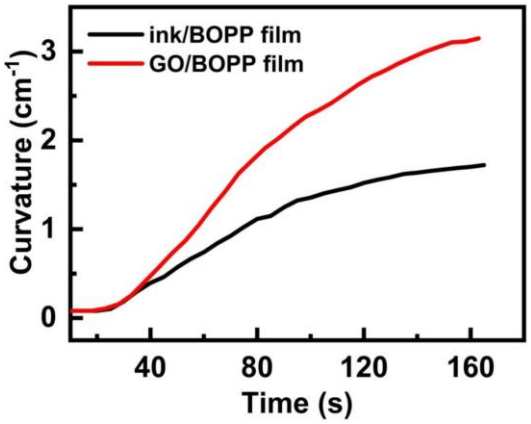

Fig. S4. Bending curvature changes of ink/BOPP and GO/BOPP films in the same humidity environment.

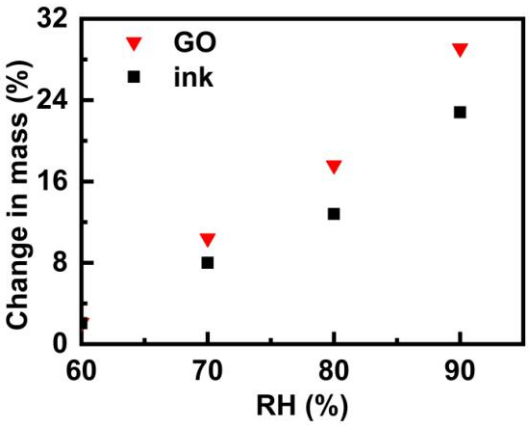

Fig. S5. Mass change of GO film and ink film as a function of RH.

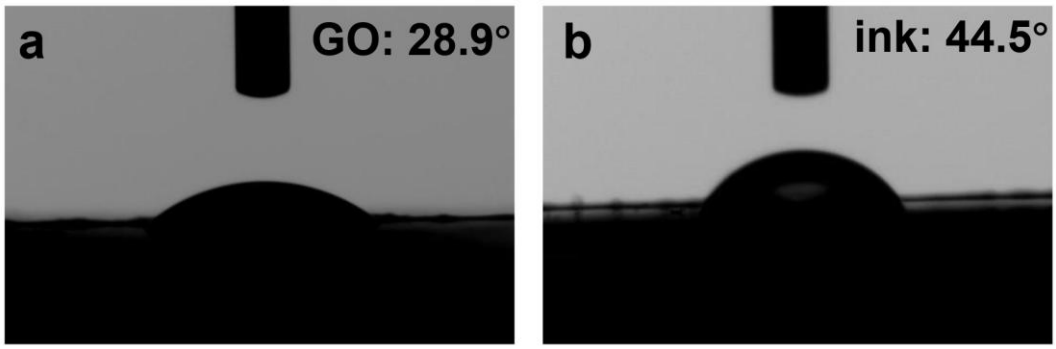

Fig. S6. Water contact angle diagrams of GO and ink films. (a) Water contact angle of GO film; (b) Water contact angle of ink film.

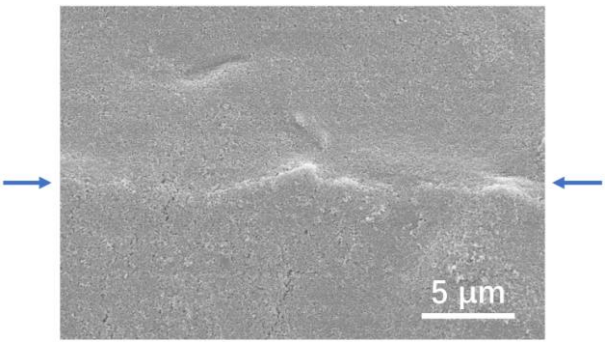

Fig. S7. SEM image showing the surface of ink layer after healing (blue arrows indicate the healed area).

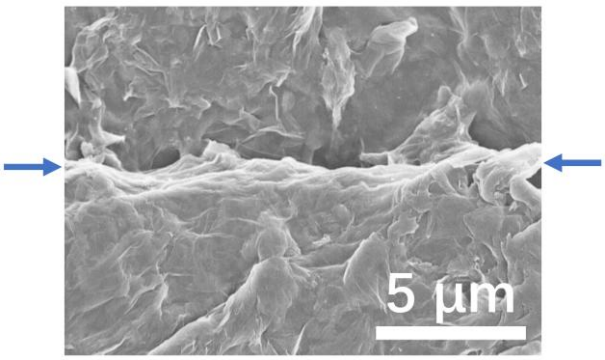

Fig. S8. SEM image showing the surface of GO layer after healing (blue arrows indicate the healed area).

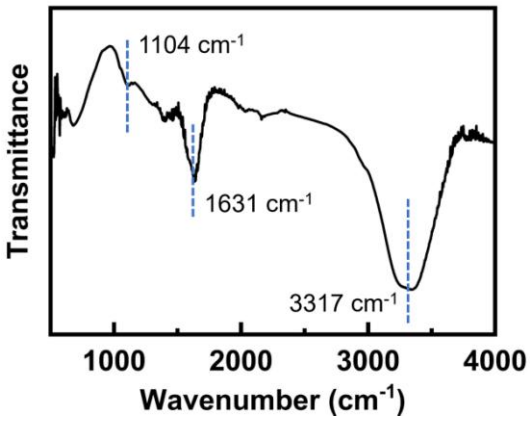

Fig. S9. FTIR spectrum of the ink film.

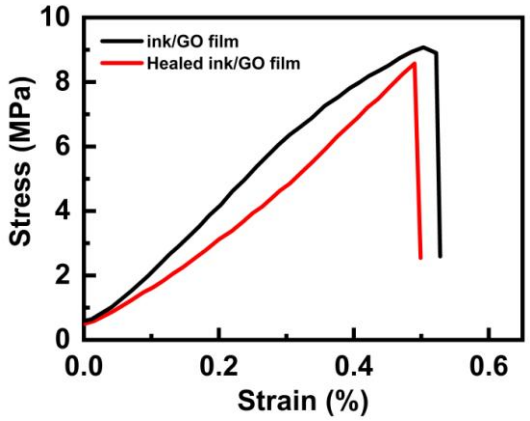

Fig. S10. Specific stress-strain curve of ink/GO composite film before cutting and after healing.

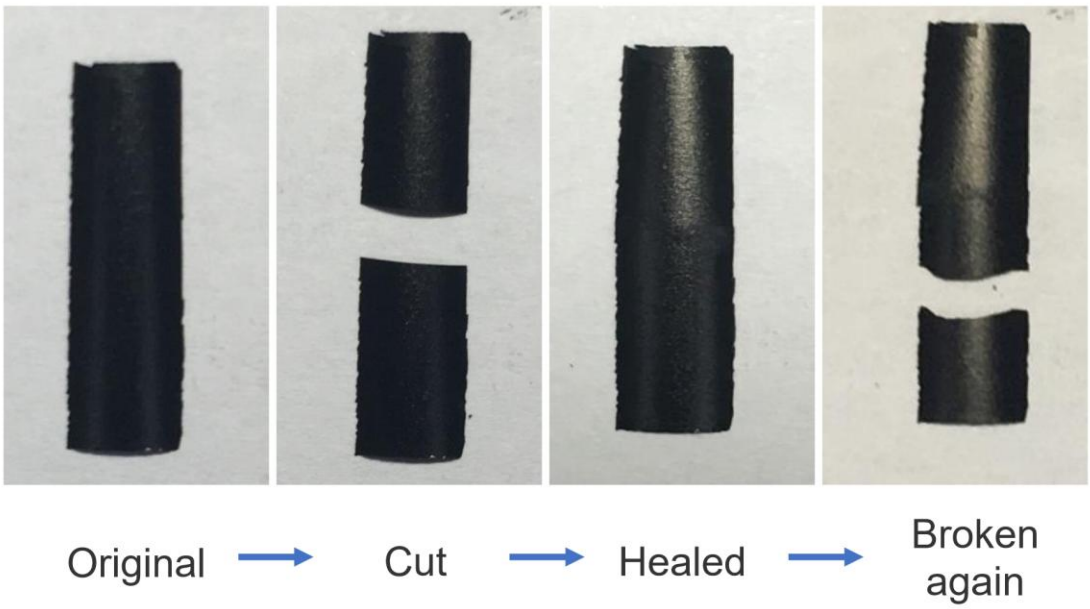

Figure. S11. The healed ink/GO film breaks at another place when being stretched.

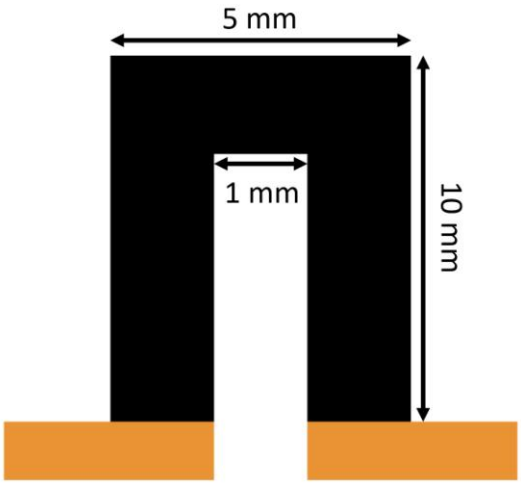

Fig. S12. Schemaic diagram of the dimensions of U-shape ink/GO actuator.

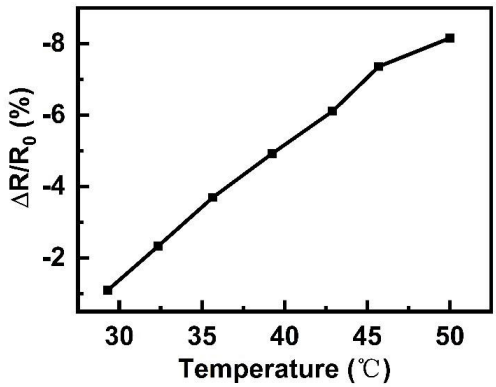

Fig. S13. Relative resistance change of the ink film as a function of temperature.

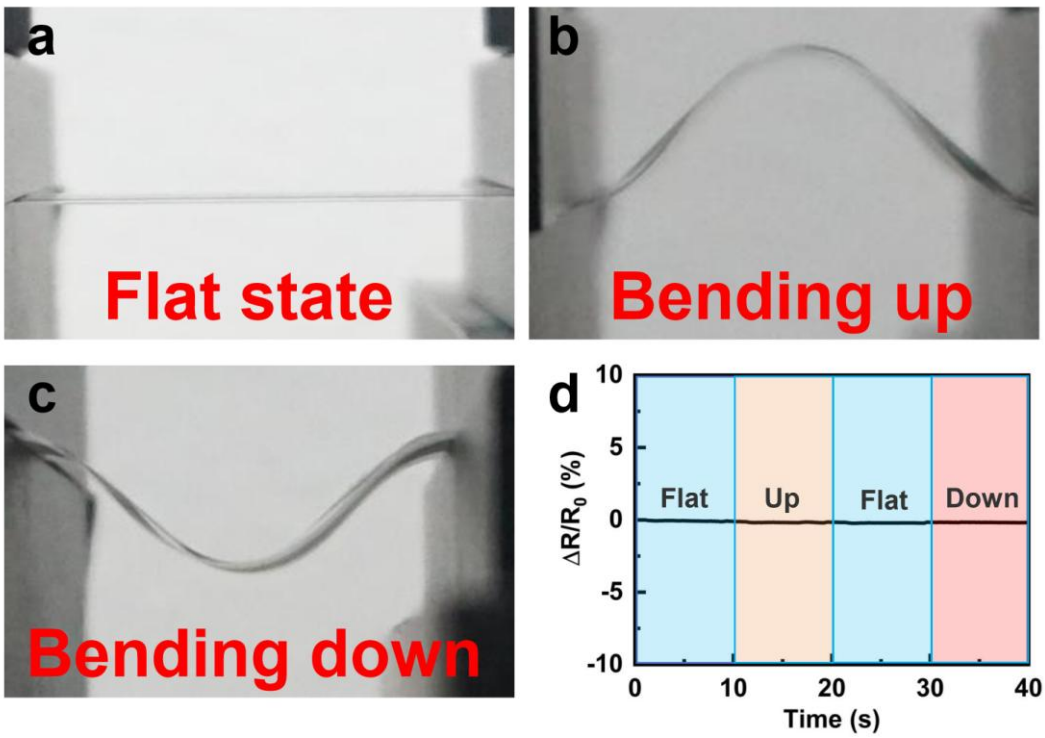

Fig. S14. Resistance change diagrams of ink/GO actuator during the passive bending process. (a) Flat state; (b) Bending up; (c) Bending down; (d) Relative resistance change of the ink/GO actuator during the bending process.

Note S1: Bending curvature calculation principle for the ink/GO actuator

Bending curvature calculation principle of the ink/GO actuator.

The parameters are defined as follows (shown in Fig. S3):

L: The length of ink/GO actuator.

r: The radius of the arc of ink/GO actuator.

x: The horizontal displacement of ink/GO actuator.

y: The vertical displacement of ink/GO actuator.

θ/2: The chord tangent angle of ink/GO actuator.

θ: The bending angle of the arc of ink/GO actuator.

The bending curvature is defined as the reciprocal of radius (*1/r*).

The chord tangent angle is given by

$$\frac{\theta}{2} = tan^{-1}\frac{x}{L-y} \qquad \text{(eq. S1)}$$

As the bending angle is given by

$$\theta = \frac{L}{r} \qquad \text{(eq. S2)}$$

The bending curvature 1/*r* is deduced as

$$\frac{1}{r} = \frac{\theta}{L}. \qquad \text{(eq. S3)}$$

Therefore, the bending curvature of the ink/GO actuator can be calculated by using the bending angle and length of the actuator.